BIOCHEMISTRY
including biophysical chemistry & molecular biology

Article

pubs.acs.org/biochemistry

Marburg Virus Glycoprotein GP2: pH-Dependent Stability of the Ectodomain α-Helical Bundle

Joseph S. Harrison,[†] Jayne F. Koellhoffer,[†] Kartik Chandran,[‡] and Jonathan R. Lai*[,†]

[†]Department of Biochemistry and [‡]Department of Microbiology and Immunology, Albert Einstein College of Medicine, 1300 Morris Park Avenue, Bronx, New York 10461, United States

Supporting Information

ABSTRACT: Marburg virus (MARV) and Ebola virus (EBOV) constitute the family *Filoviridae* of enveloped viruses (filoviruses) that cause severe hemorrhagic fever. Infection by MARV requires fusion between the host cell and viral membranes, a process that is mediated by the two subunits of the envelope glycoprotein, GP1 (surface subunit) and GP2 (transmembrane subunit). Upon viral attachment and uptake, it is believed that the MARV viral fusion machinery is triggered by host factors and environmental conditions found in the endosome. Next, conformational rearrangements in the GP2 ectodomain result in the formation of a highly stable six-helix bundle; this refolding event provides the energetic driving force for membrane fusion. Both GP1 and GP2 from EBOV have been extensively studied, but there is little information available for the MARV glycoproteins. Here we have expressed two variants of the MARV GP2 ectodomain in *Escherichia coli* and analyzed their biophysical properties. Circular dichroism indicates that the MARV GP2 ectodomain adopts an α-helical conformation, and one variant sediments as a trimer by equilibrium analytical ultracentrifugation. Denaturation studies indicate the α-helical structure is highly stable at pH 5.3 (unfolding energy, $\Delta G_{unf,H_2O}$, of 33.4 ± 2.5 kcal/mol and melting temperature, T_m, of 75.3 ± 2.1 °C for one variant). Furthermore, we found the α-helical stability to be strongly dependent on pH, with higher stability under lower-pH conditions (T_m values ranging from ∼92 °C at pH 4.0 to ∼38 °C at pH 8.0). Mutational analysis suggests two glutamic acid residues (E579 and E580) are partially responsible for this pH-dependent behavior. On the basis of these results, we hypothesize that the pH-dependent folding stability of the MARV GP2 ectodomain provides a mechanism for controlling conformational preferences such that the six-helix bundle "postfusion" state is preferred under conditions of appropriately matured endosomes.

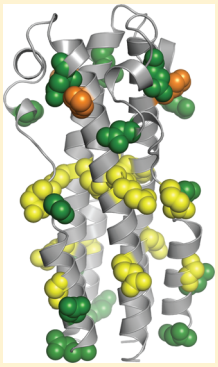

Marburg virus (MARV) and the related Ebola virus (EBOV) belong to the family *Filoviridae* of enveloped viruses that cause a rapidly progressing hemorrhagic fever with human case fatalities of 50−90%.[1,2] Similar to infection with other enveloped viruses, infection with MARV requires coordinated conformational changes in the envelope glycoproteins that ultimately result in fusion between the viral and cellular membranes.[3−6] The envelope glycoprotein spike of MARV and EBOV consists of three copies each of a surface subunit (GP1) and a transmembrane subunit (GP2) that anchors the spike to the viral membrane.[3,5,7−11] Structural and biochemical work with EBOV GP1 and GP2 has demonstrated that, prior to membrane fusion, the viral particle must first be internalized into cellular endosomes or lysosomes where host cysteine proteases cathepsins L and B (CatL and CatB, respectively) remove all but a small (∼17 kDa) portion of GP1.[7,8,12−14] Host factors are then proposed to trigger the fusion reaction, possibly by interaction with the remaining fragment of GP1. Recent reports have demonstrated that the endosomal cholesterol transporter Niemann Pick C1 (NPC-1) is critical for EBOV entry, and other unidentified factors may also be required.[15,16] The GP2 subunit contains two heptad repeat regions in the ectodomain [N- and C-terminal (NHR and CHR, respectively)] that fold into a stable six-helix bundle. Therefore, the postulated EBOV fusion mechanism is similar to that of HIV-1 gp41 and other members of the structurally defined "class I" family of envelope glycoproteins.[3−6,9−11] In this model, the N-terminal portion of GP2, which contains a fusion loop, embeds in the host cell membrane following binding of the receptor to cleaved GP1. This conformational change in GP2 gives rise to a transient intermediate known as the "prehairpin" or "extended" intermediate in which the NHR and CHR are exposed to the extraviral environment. Next, folding of the GP2 six-helix bundle provides the driving force for membrane fusion by pulling the virus and host cell membranes into the proximity of each other. The events leading to MARV membrane fusion are presumably similar, because sequences of GP1 and GP2 are highly conserved among these two viruses.[17,18] However, few biochemical studies of the MARV glycoproteins have been reported to date.

The envelope glycoproteins of many viruses that enter the cell via the endosome contain structural elements that drastically affect the stability of the prefusion conformation (the spike) or the postfusion conformation in a pH-dependent manner.[4−6,19−26] In these cases, protonation of one or more side chains drives conformational preferences toward active

Received: January 10, 2012
Revised: February 27, 2012
Published: February 27, 2012

   dx.doi.org/10.1021/bi3000353 | *Biochemistry* 2012, 51, 2515−2525

fusogenic states at low pH.[21−24] This feature provides a general mechanism for controlling membrane fusion such that it is triggered only when the virus is present in an appropriately matured endosome. For example, low-pH-induced conformational changes in the envelope glycoprotein of influenza A virus (HA) result in the exposure of the fusion loop and ultimately its insertion into the host membrane.[19,20] However, the precise residues that are responsible for this transformation vary among strains.[27] In the alphavirus Semliki Forest virus (SFV), the prefusion spike consists of two glycoproteins, E1 and E2, which form a fusion-inactive heterodimer.[22−24] Protonation of conserved histidine residues in both subunits destabilizes the E1−E2 homodimer and promotes formation of an E1 trimer, the active fusogenic form of the envelope glycoprotein. In EBOV entry, an acidic pH is required to activate CatL and CatB, which have optimal catalytic activity at pH ∼5 and whose proteolysis of GP1 is an essential step for infection.[12,13] We recently demonstrated that the folding stability of designed proteins modeled after the six-helix bundle of EBOV GP2 is dependent on pH, with higher stability at lower pH, suggesting that the pH alters conformational preferences of the NHR and CHR.[28] It has been recently reported that peptides corresponding to the fusion loop of EBOV GP2 undergo pH-dependent structural changes that result in an increase in fusogenic activity at low pH.[29] Furthermore, the proteolytically primed form of the GP1−GP2 spike assembly can be activated to bind lipids by treatment with acidic pH or mild reductants.[30] Together, these findings suggest a model for EBOV membrane fusion in which the acidification of endosomal compartments triggers the fusogenic machinery of the viral envelope spike.

Here we describe the expression, purification, and initial biophysical characterization of the GP2 ectodomain from MARV. We found that the MARV GP2 ectodomain forms an α-helical trimer, suggesting a membrane fusion mechanism similar to that of EBOV. Furthermore, we found the stability of the MARV α-helical bundle to be pH-sensitive, with much higher stability under acidic conditions. We performed site-directed mutagenesis to identify residues that are responsible for this behavior. Variants containing mutations to several acidic residues in the NHR core trimer and on the external CHR α-helices were characterized and some were found to have altered pH-dependent stability. These results suggest that membrane fusion in MARV may also be controlled by the pH-dependent stability of the postfusion conformation.

MATERIALS AND METHODS

Cloning, Expression, Purification, and Refolding of the MARV GP2 Ectodomain. A synthetic DNA fragment encoding "MarVGP2-C" (see Results) with an N-terminal hexahistidine tag was obtained from a commercial supplier (Genewiz, South Plainfield, NJ). This gene was cloned into pET22b (Novagen, Madison, WI) with NdeI and XhoI restriction sites to produce expression plasmid pJH4. Site-directed mutagenesis was performed to introduce a C557S mutation to yield expression plasmid pJH5 (encoding "MarVGP2-S"). Expression, purification, and refolding of MarVGP2-C and MarVGP2-S were similar. *Escherichia coli* BL21 (Invitrogen, Carlsbad, CA) cells harboring pJH4 or pJH5 were grown in LB broth at 37 °C to an OD_{600} of ∼0.6, and protein expression was induced by addition of 1 mM isopropyl β-D-1-thiogalactopyranoside (IPTG). The culture was incubated at 37 °C for an additional 14−16 h. Cells were harvested by centrifugation and lysed by being stirred in 6 M guanidine hydrochloride (GdnHCl) for 3 h at room temperature. The cell debris was pelleted by ultracentrifugation, and the supernatant was applied directly to Ni-NTA resin (Qiagen, Valencia, CA). The resin was washed with 10 column volumes of phosphate-buffered saline (PBS) containing 6 M GdnHCl and 50 mM imidazole, and then the MarVGP2-C or MarVGP2-S protein was eluted with PBS containing 6 M GdnHCl and 250 mM imidazole. The eluted protein was concentrated and then further purified by reverse-phase high-performance liquid chromatography on a Vydac (Hesperia, CA) C18 column (10 μM, 250 mm × 21.2 mm) with water/acetonitrile/trifluoroacetic acid mobile phases. Fractions containing pure protein were pooled, lyophilized, and redissolved in 6 M GdnHCl. The proteins were refolded by stepwise dialysis first into 100 mM glycine hydrochloride (pH 3.5) and then into 10 mM sodium acetate (pH 5.3). Protein concentrations were kept below 0.5 mg/mL during the refolding process. The precipitated material was removed by centrifugation and the refolded protein used immediately for analysis or flash-frozen and stored at −80 °C.

Circular Dichroism (CD) Spectroscopy. Measurements were performed on a Jasco J-815 spectrometer with a 1 cm quartz cuvette. Protein concentrations ranged from 1 to 4 μM as determined by the absorbance at 280 nm. Circular dichroism wavelength scans were obtained with a 1 nm step size and a 2 s averaging time. The signal was converted to mean molar ellipticity (θ) using the equation $\theta = (100\varepsilon)/(nl[P]_{tot})$, where ε is the raw CD signal in degrees, n is the number of amide chromophores, l is the path length, and $[P]_{tot}$ is the protein concentration.[31]

Chemical and thermal denaturation was monitored at 222 nm (θ_{222}). For chemical denaturation, protein samples were diluted into the appropriate analysis buffer containing varying amounts of GdnHCl, the solution was allowed to equilibrate for 1 min, and then θ_{222} was determined. The data were plotted as a function of GdnHCl concentration, corrected for the baseline in folded and unfolded states, and then converted to fraction unfolded (F_{unf}) using the expression $(\theta_{222} - \theta_U)/(\theta_F - \theta_U)$, where θ_F and θ_U are the CD signals for the folded and unfolded states, respectively. The ΔG_{unf} at each GdnHCl concentration was calculated using a monomer−trimer model ($3M_U \leftrightarrow T_F$, where M_U is the unfolded monomer and T_F is the folded trimer): $\Delta G_{unf} = RT \ln[(3F_{unf}^3[P]_{tot}^2)/(1 - F_{unf})]$, where R is the gas constant and T is the absolute temperature.[32] The unfolding energy in water ($\Delta G_{unf,H_2O}$) was estimated by linear extrapolation to 0 mM GdnHCl using points in the transition region.[33] Thermal denaturation data were obtained with a 3−5 °C step size and equilibration for 2 min at each temperature. θ_{222} was plotted as a function of temperature, corrected for the baseline, and converted to F_{unf}. The data were fit to a standard four-parameter logistic equation, and the melting temperature, T_m, was obtained from the inflection point of the curve.

Equilibrium Analytical Ultracentrifugation (AU). Analysis was performed on a Beckman XL-1 analytical ultracentrifuge with a Ti60 rotor. Samples of MarVGP2-S were loaded into 1.2 cm cells at a protein concentration of 20 μM, and storage buffer that did not contain protein was used in the reference cell. Equilibrium sedimentation experiments were conducted at rotor speeds of 12K and 19K rpm. At each rotor speed, samples were allowed to equilibrate for 24 h and the radial spectra collected at 230 nm. Comparison of overlaid spectra indicated that there was no mass depletion. The data from both rotor speeds were fit globally to a single-ideal species model using Heteroanalysis (Biotechnology/Bioservices Cen-

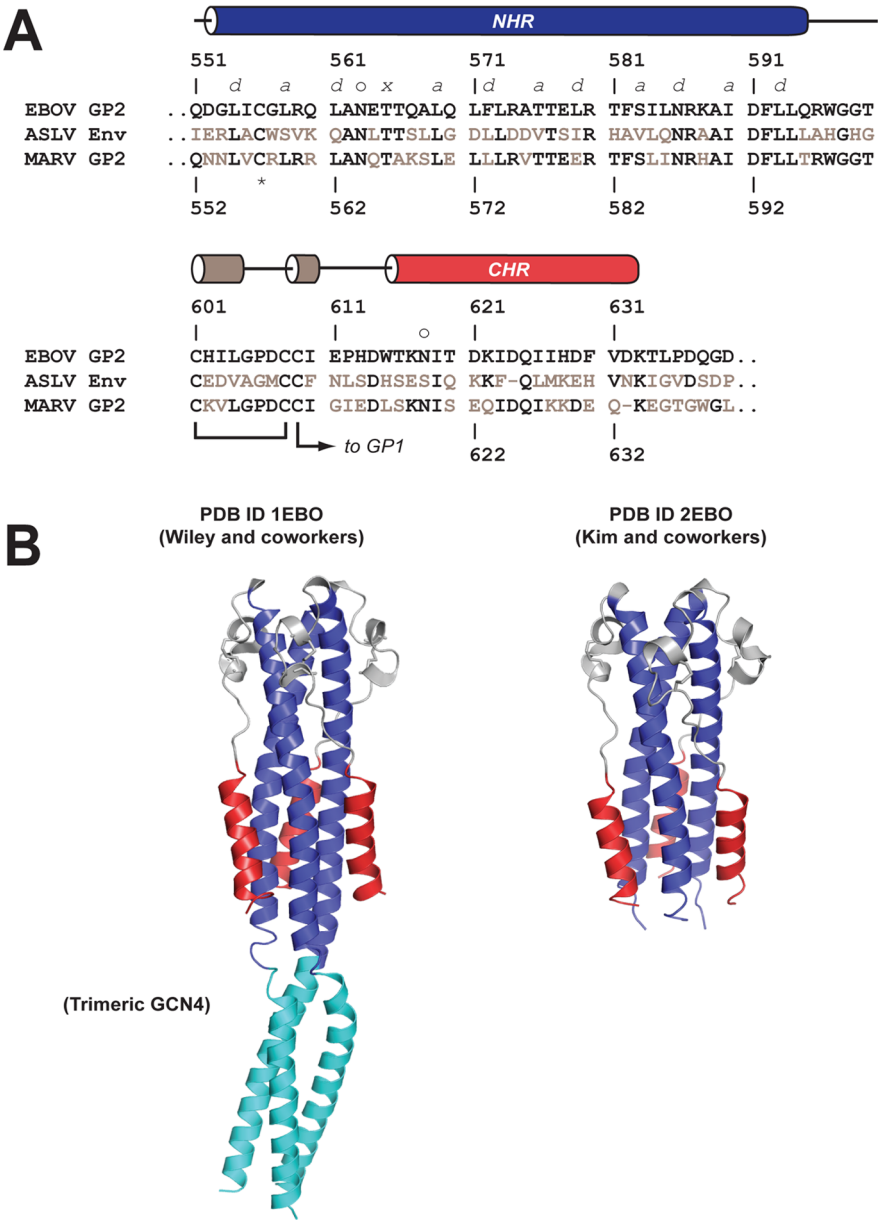

Figure 1. (A) Sequence alignment of GP2 from *Zaire ebolavirus* (EBOV), ASLV, and MARV (residues that differ from those of EBOV colored gray). The amino acid numbering for EBOV GP2 and MARV GP2 differs by 1; the EBOV numbering is shown above the sequence alignment and the MARV numbering below. The regions corresponding to the NHR, CHR, and helix−turn−helix regions of EBOV GP2 are indicated with cylinders whose colors match the structural elements depicted in panel B. Established disulfide bond connectivities are shown, and glycosylation sites are denoted with an o. The T565 (EBOV numbering) residue that gives rise to the unusual 3-4-4-3 hydrophobic stutter in the NHR is denoted with an x; other residues in the NHR that form core positions are denoted *a* and *d*. The C556 (EBOV numbering) residue in NHR is denoted with an asterisk (below). (B) Crystal structures of the EBOV GP2 ectodomain reported by Wiley and co-workers[10] (PDB entry 1EBO) and Kim and co-workers[11] (PDB entry 2EBO). In the Wiley structure, the trimeric GCN4 tag is colored cyan.

ter, University of Connecticut, Storrs, CT). Nonlinear regression was performed in accordance with the expression $c_r = c_o \exp[M(1 - \upsilon\rho)\omega^2(r^2 - r_o^2)/2RT]$ + base, where c_r is the concentration (in absorbance units) at radial position r, c_o is the concentration at an arbitrary reference position r_o near the meniscus, υ is the partial specific volume, ρ is the solvent density, ω is the rotor speed, R is the gas constant, T is the absolute temperature, and base is a baseline absorbance correction to account for nonsedimenting species.[34] Molecular weight estimates were obtained from the parameter M. Fits were judged to be adequate if there was no systematic deviation of residuals. A partial specific volume of 0.7337 mL/g was calculated for MarVGP2-S based on amino acid composition, and a solvent density of 1.00182 g/mol was estimated using Sednterp (University of New Hampshire, Durham, NH).

Structural Modeling and Site-Directed Mutagenesis. A structural homology model of the MARV GP2 ectodomain was generated using the SWISS-MODEL server (http://swissmodel.expasy.org/) with the alignment shown in Figure 1A and Protein Data Bank (PDB) entry 2EBO as a template.[11] This structural model was used to identify positions for analysis by site-directed mutagenesis. Mutant MarVGP2-C or MarVGP2-S clones were prepared using the following protocol. Briefly, pJH4 or pJH5 DNA served as the template for

dx.doi.org/10.1021/bi3000353 | *Biochemistry* 2012, 51, 2515−2525

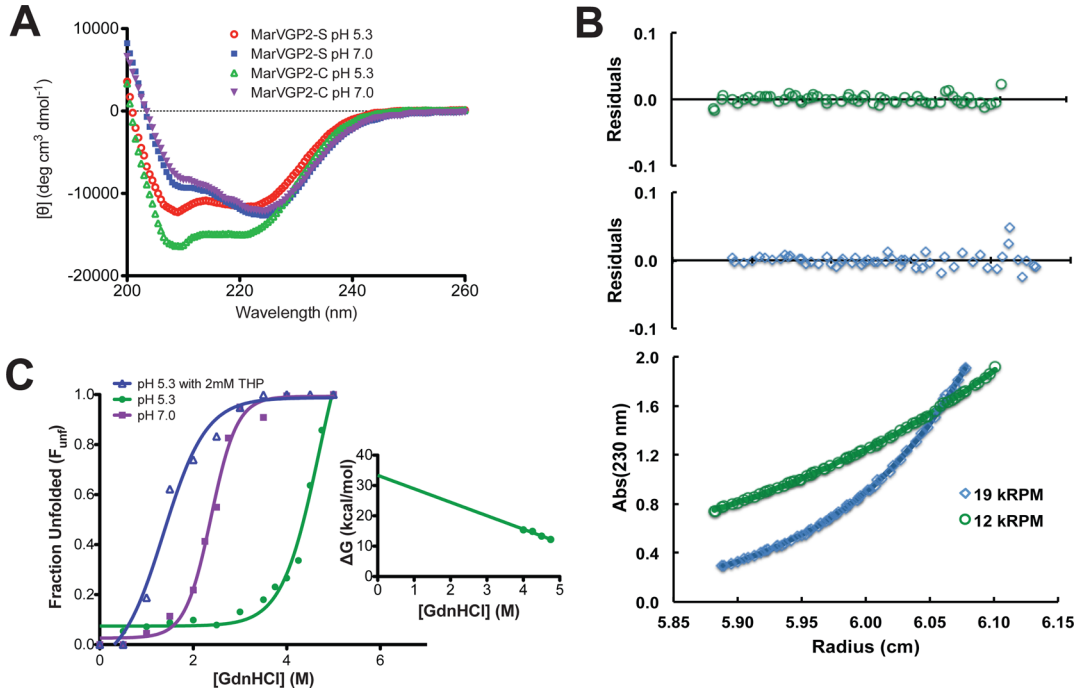

Figure 2. Biophysical characterization of the MARV GP2 ectodomain. (A) CD spectra of MarVGP2-S in 10 mM sodium acetate (pH 5.3) and 10 mM sodium phosphate (pH 7.0). (B) Representative analytical ultracentrifugation at pH 5.3. High-resolution data were obtained at rotor speeds of 12 and 19 kRPM and fit to a single-ideal species model to yield a molecular mass estimate consistent with a trimer (see the text). (C) GdnHCl denaturation of MarVGP2-S in 10 mM NaOAc (pH 5.3) in the absence and presence of the reducing agent THP and in 20 mM NaH_2PO_4 (pH 7.0). The denaturant midpoint (C_m) values are 4.7 ± 0.2 M GdnHCl at pH 5.3, 1.4 ± 0.1 M GdnHCl at pH 5.3 with THP, and 2.4 ± 0.1 M GdnHCl at pH 7.0. Linear extrapolation of the pH 5.3 data yielded a $\Delta G_{unf,H_2O}$ of 33.4 ± 2.5 kcal/mol (inset).

oligonucleotide-based plasmid replication using the primers containing the desired substitutions. Following DNA synthesis, the template DNA was destroyed by digestion with DpnI for 3 h at 37 °C, and *E. coli* XL1-Blue cells (Stratagene, La Jolla, CA) were transformed with the resulting mixture. Clones were screened by sequence analysis, and those that contained the desired mutations were used for protein production. The preparation of mutant proteins was similar to that for wild-type MarVGP2-C and MarVGP2-S (described above) and generally had comparable yields.

RESULTS

Predicted Six-Helix Bundle of the Marburg Virus GP2 Ectodomain. To define the MARV GP2 six-helix bundle, we compared its ectodomain sequence to that of the EBOV (*Zaire* strain) GP2 ectodomain and the structurally related avian sarcoma/leukosis virus (ASLV) Env ectodomains (Figure 1A).[9−11,35,36] The crystal structures for two variants of the EBOV GP2 ectodomain in the postfusion state were described previously by Wiley and co-workers (PDB entry 1EBO)[10] and Kim and co-workers (PDB entry 2EBO)[11] (Figure 1B). The EBOV GP2 ectodomain adopts a six-helix bundle with a long, central trimeric coiled-coil core consisting of the NHR segment and three shorter CHR α-helices arranged in an antiparallel configuration about the periphery of the NHR core trimer. An intervening loop region contains a short helix−turn−helix segment that is stabilized by an intramolecular disulfide bond between C601 and C608. The Wiley EBOV GP2 structure contained a trimeric GCN4 segment N-terminal to the NHR to promote solubility and expression.[9,10] On the basis of the alignment with EBOV GP2 and analysis of these structures, we predicted that a fragment consisting of residues 553−633 of MARV GP2 would adopt a stable six-helix bundle, with residues 553−596 forming the NHR core trimer, residues 597−615 forming the loop, and residues 616−633 forming CHR (note the amino acid numbering for EBOV GP2 and MARV GP2 differs by 1; the numbering for both proteins is shown in Figure 1A). This fragment encompasses the majority of the ectodomain but lacks the fusion loop and the membrane-proximal external region.

Previous work with EBOV GP2 and ASLV Env established disulfide bond connectivity of the three cysteines located at positions 601, 608, and 609 (positions 602, 609, and 610, respectively, in MARV GP2).[9−11,35,36] Residues C601 and C608 in EBOV GP2 form the intramolecular linkage that stabilizes the helix−turn−helix region of the loop between the NHR and CHR, and C609 participates in an intermolecular bridge that tethers GP2 to the surface subunit (GP1).[8] However, both C608 and C609 can both form disulfide bonds with C601 in the isolated EBOV GP2 ectodomain.[9−11] Therefore, we incorporated a C610S mutation (this position is predicted to participate in the disulfide bond with GP1) into our MARV GP2 design to prevent heterogeneous disulfide bond formation. Residue C556 is predicted to lie in the α-helical NHR region in the EBOV GP2 postfusion conformation,[10] but this residue participates in a disulfide bridge with C511 to stabilize an antiparallel β-sheet in the prefusion conformation.[8] The segment between C511 and C556 (EBOV numbering) is well-conserved among filoviruses and is thought to correspond to the fusion loop.[8] Residue C556 was replaced with aspartic acid in the Wiley EBOV GP2 construct and with alanine in the Kim EBOV GP2 construct.[10,11] We prepared two constructs of the MARV GP2 ectodomain: one in which the analogous wild-type C557 side chain was preserved

dx.doi.org/10.1021/bi3000353 | *Biochemistry* 2012, 51, 2515−2525

(MarVGP2-C) and a second containing a C557S mutation (MarVGP2-S).

A "stutter" in the periodicity of the NHR heptad repeat pattern was observed in the EBOV GP2 postfusion conformation.[9−11] Residue T565 points toward the core of the NHR trimer but occupies a position that, along with the surrounding core NHR residues, results in an unusual 3-4-4-3 hydrophobic repeat (the canonical heptad repeat has a 3-4-3-4 periodicity). This stutter causes a slight distortion of the EBOV NHR α-helix; the alignment in Figure 1A indicates that such a stutter also exists in MARV GP2 (T566) and is included in both MarVGP2-C and MarVGP2-S constructs.

Purification and Characterization of MarVGP2-C and MarVGP2-S. MarVGP2-C and MarVGP2-S proteins were isolated from *E. coli* and refolded by stepwise dialysis first into 100 mM glycine hydrochloride (pH 3.5) and then into 10 mM sodium acetate buffer (pH 5.3). A portion of protein in each case precipitated during the refolding process; this aggregation could be controlled to some extent by maintaining low protein concentrations (<0.5 mg/mL). Despite this aggregation, we recovered a reasonable yield of soluble, refolded material through this procedure (~0.1 mg/L of culture). The final refolding buffer did not contain reducing agent, which allowed disulfide bonds to form between C602 and C609 (which stabilizes the helix−turn−helix segment). Sodium dodecyl sulfate−polyacrylamide gel electrophoresis (SDS−PAGE) analysis under reducing and nonreducing conditions indicated a significant proportion of MarVGP2-C existed as disulfide-bonded oligomers, likely via cross-links between the unpaired C557 residue on individual chains (see the Supporting Information). In contrast, such cross-linked species were not abundantly observed in MarVGP2-S.

Circular dichroism indicates that both MarVGP2-C and MarVGP2-S are α-helical with double minima at 208 and 222 nm in 10 mM sodium acetate (pH 5.3) (Figure 2A). Analytical ultracentrifugation studies under similar conditions at 20 μM indicate that MarVGP-S sediments as a single ideal species with a molecular mass of 34250 ± 280 Da (Figure 2B), consistent with a stable trimer (expected trimer molecular mass of 33260 Da). We therefore conclude that MarVGP2-S forms a six-helix bundle, similar to the corresponding regions of the EBOV GP2 postfusion conformation.[9−11] To estimate the folding stability of MarVGP2-S, we performed chemical denaturation with GdnHCl (Figure 2C). This analysis yielded a $\Delta G_{unf,H_2O}$ of 33.4 ± 2.5 kcal/mol when fit to a monomer−trimer model at pH 5.3.[32] To determine whether disulfide bonding between the C602 and C609 contributed to this stability, we performed the GdnHCl denaturation in the presence of the reducing agent tris(hydroxypropyl)phosphine (THP, 2 mM) and found that the protein was markedly destabilized under reducing conditions. The denaturant midpoint, C_m, was 4.7 ± 0.2 M GdnHCl without THP and 1.4 ± 0.1 with THP. This result indicates that the MARV GP2 C602−C609 disulfide bond was oxidized during the refolding protocol and is consistent with observations that the EBOV GP2 ectodomain is stabilized by disulfide bridges between the corresponding C601 and C608 residues.[11] In EBOV GP2, the established disulfide bond connectivity of the C601−C608 bond was determined by stability studies with a C609A mutant (which would form an obligate C601−C608 disulfide bond) and a C608A mutant (obligate C601−C609 disulfide bond).[11] The C601−C608 disulfide variant displayed enhanced stability relative to the C601−C609 disulfide variant. We did not examine a C602−C610 disulfide variant of MarVGP2-S; however, the highly stable nature of the MarVGP2-S α-helical structure suggests the C602−C609 disulfide bonding pattern is also relevant in MARV GP2.

pH-Dependent Stability. We examined the CD spectra of MarVGP2-S and MarVGP2-C under various buffering conditions and found that the ratio of peaks at 208 and 222 nm varied with pH for both proteins (wavelength scans at pH 5.3 and 7.0 are shown in Figure 2A). Strong 222 nm signals were observed at pH 5.3 and 7.0, indicating significant α-helical character under both of these conditions. However, the relative intensities of the 208 and 222 nm peaks varied with pH, suggesting differences in quaternary packing of α-helical segments.[37]

To further explore pH-dependent structural effects, we performed thermal denaturation of MarVGP2-S and MarVGP2-C under buffering conditions ranging from pH 4.0 to 8.0 using the 222 nm CD signal to monitor folding (Figure 3

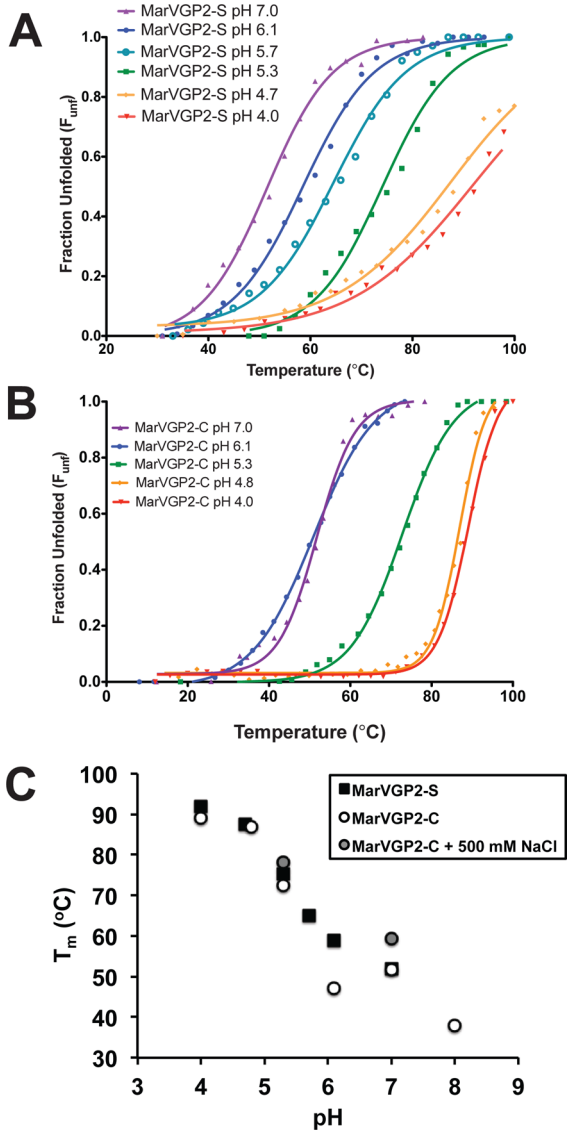

Figure 3. pH-dependent thermal stability of the MARV GP2 α-helical bundle as monitored by θ_{222}. Thermal denaturation curves of MarVGP2-S (A) and MarVGP2-C (B) under various buffering conditions. (C) Plot of T_m vs pH.

dx.doi.org/10.1021/bi3000353 | *Biochemistry* 2012, 51, 2515−2525

and Table 1). We found that the melting temperature (T_m), which provides an estimate of overall folding stability, was

Table 1. Stabilities of MarVGP2-S and MarVGP2-C under Various Buffering Conditions

buffering condition	T_m (°C)[a]
MarVGP2-S	
10 mM NaOAc, pH 4.0	~92[b]
10 mM NaOAc, pH 4.7	~88[b]
10 mM NaOAc, pH 5.3	75.3 ± 2.1
10 mM NaOAc, pH 5.7	65.1 ± 1.0
10 mM NaOAc, pH 6.1	58.8 ± 1.1
20 mM $NaHPO_4$, pH 7.0	51.8 ± 0.4
MarVGP2-C	
10 mM NaOAc, pH 4.0	89.0 ± 0.2
10 mM NaOAc, pH 4.8	86.9 ± 0.3
10 mM NaOAc, pH 5.3	72.4 ± 1.4
10 mM NaOAc, pH 6.1	47.0 ± 1.5
20 mM $NaHPO_4$, pH 7.0	51.6 ± 1.3
20 mM $NaHPO_4$, pH 8.0	~38[c]
10 mM NaOAc, pH 5.3, 500 mM NaCl	78.2 ± 3.0
20 mM $NaHPO_4$, pH 7.0, 500 mM NaCl	59.3 ± 1.0

[a]Errors listed here represent 95% confidence intervals from data fitting. [b]Complete unfolding was not observed at 100 °C; an estimate for T_m based on fitting the partial unfolding curve is provided. [c]A broad thermal transition prevented accurate determination of T_m.

sensitive to pH in this range. In 10 mM sodium acetate, MarVGP2-S could not be completely unfolded at pH 4.0 and 4.7 (T_m values estimated to be ~92 and ~88 °C, respectively, based on partial unfolding curves), consistent with a highly stable α-helical bundle. However, at pH 5.3, full denaturation was observed with a T_m of 75.3 ± 2.1 °C, indicating that the unfolding stability is much lower at this pH than at pH 4.0 and 4.7. At pH 6.1 (10 mM NaOAc buffer) and pH 7.0 (20 mM NaH_2PO_4 buffer), the T_m values were significantly lower (58.8 ± 1.1 and 51.8 ± 0.4 °C, respectively). Similar trends were observed for MarVGP2-C, with T_m values ranging from 89.0 ± 0.2 °C at pH 4.0 to ~38 °C at pH 8.0 (Figure 3B and Table 1). Figure 3C shows T_m as a function of pH for both MarVGP2-S and MarVGP2-C. Overall, the structural stability of the ectodomain is significantly higher at lower pH values, with an ~50 °C difference in T_m over the range of pH 4.0−8.0. The pH-dependent stability of MarVGP2-S was confirmed by GdnHCl denaturation (Figure 2C); the C_m was significantly higher at pH 5.3 (4.7 ± 0.2 M GdnHCl) than at pH 7.0 (2.4 ± 0.1 M GdnHCl).

In the GP2 ectodomain structures from EBOV, a conserved central asparagine (N586) in the NHR points toward the center of the core and binds monovalent anions.[10,11] This anion-binding pocket was also observed in the ectodomain of murine moloney leukemia virus (MoMLV), which is structurally similar to EBOV GP2 despite being from a phylogenetically unrelated virus.[38] The sequence alignment suggests a similar pocket exists in MARV GP2 (N587). In EBOV GP2, the presence and nature of the monovalent ion were reported to have moderate effects on thermal stability (the reported T_m values were 84 °C in the presence of 5 mM NaCl or NaBr, 79 °C in the presence of 5 mM NaF, and 77 °C without salt).[11] Although the data in Figure 3 and Table 1 were obtained in buffer that did not contain salt and protein samples were exhaustively dialyzed during the refolding process, we cannot rule out the possibility that trace monovalent anions affected the determinations of T_m under various buffering conditions. However, the observed T_m values under various buffering conditions spanned a range of ~50 °C, a range much larger than that previously observed with salt effects in EBOV GP2 (range of ~8 °C).[11] At both pH 5.3 and 7.0, we observed an increase in T_m for MarVGP-C upon addition of 500 mM NaCl to the solution [ΔT_m values of 5.8 °C at pH 5.3 and 7.7 °C at pH 7.0 (Figure 3C and Table 1)]. However, the stabilization was relatively minor in comparison to the change in stability among the various pH conditions. Furthermore, the T_m at pH 5.3 in the presence of 500 mM NaCl was 18.9 °C higher (78.2 ± 3.0 °C) than that at pH 7.0 with an equivalent amount of salt (59.3 ± 1.0 °C). Therefore, we conclude that the effects of salt on stability are relatively minor in comparison to the effects of pH.

These results suggest that the stability of the MARV GP2 six-helix bundle is sensitive to pH, possibly by protonation of side chain groups. The stabilization of the structure at high salt concentrations may also indicate that charge screening increases the stability of the six-helix bundle, further implicating the interaction between ionic groups controls the pH-dependent stability. The pH range of the transition from highly stable (pH 4) to moderately stable (pH 7) occurs in a range that is consistent with pH-dependent stability mediated by acidic residues (Glu and Asp) or histidine residues in the influenza, SFV, and VSV glycoproteins.[19−26] Similar phenomena were observed in designed protein mimics of the EBOV GP2 α-helical bundle; in this case, the pH-dependent stability was in part due to acidic residues that, when deprotonated, are predicted to disfavor the α-helical bundle formation.[28] Mutational studies of the disulfide-containing loop of ASLV Env suggest that this region may play a role in pH-dependent conformational changes for that system.[36] Furthermore, the recently reported structure of GP2 from an arenavirus suggests that many intrachain salt bridges stabilize the postfusion conformation.[39]

Structural Homology Model and Mutagenesis. We generated a structural homology model of the MARV GP2 ectodomain based on the structure and alignment of the EBOV ectodomain in an attempt to determine which residues might be responsible for the pH-dependent stability (Figure 4). The MARV GP2 ectodomain contains six total glutamic acid residues, five aspartic acid residues, and a single histidine residue (these ionizable side chains are shown in space-filling mode in Figure 4A). We identified three putative side chain−side chain interactions that could potentially contribute to pH-dependent behavior (Figure 4B−D). Residue E580 in MARV corresponds to a heptad repeat core residue L579 in the HR1 of EBOV; the MARV GP2 structural homology model predicts the side chain of this glutamic acid residue is oriented toward the core of the trimer (Figure 4B).[10,11] We hypothesized that this residue may be responsible for the pH-dependent stability because, if it is deprotonated, juxtaposition of E580 anionic side chains from opposing monomers to form the central NHR coiled coil would be unfavorable. Similar interactions between acidic residues are observed at the low-pH-dependent trimer interface of VSV G.[26] Variants of the homodimeric coiled-coil GCN4 containing an aspartic acid residue at a core *a* position exhibit similar pH-dependent effects.[40] At the surface of the model, the side chain of E579 on the NHR (E578 in EBOV) is predicted to be near E614 in the loop region (H613 in EBOV) (Figure 4C). Contacts between acidic side chains are also

dx.doi.org/10.1021/bi3000353 | *Biochemistry* 2012, 51, 2515−2525

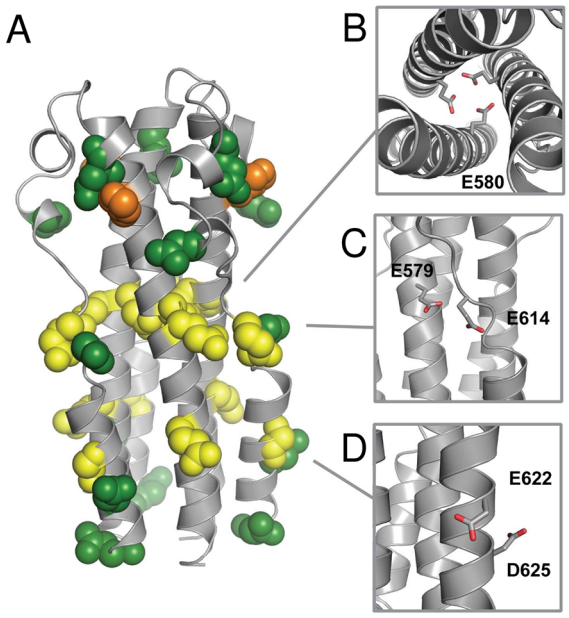

Figure 4. (A) Structural homology model of the MARV GP2 ectodomain based on the crystal structure of EBOV GP2[11] (PDB entry 2EBO). Glutamic acid (yellow), aspartic acid (green), and histidine (orange) residues are shown in space-filling mode. (B–D) Predicted interactions that could destabilize the six-helix bundle, shown as sticks and colored by atom for the sake of clarity: (B) E580 interactions in the NHR core trimer, (C) E579–E614 interaction between opposing monomers, and (D) E622–D625 $i \rightarrow i + 3$ intrahelical interaction.

observed in the low-pH coiled coils of VSV G and influenza HA.[20,26] Furthermore, E622 (D621 or N621 in EBOV, depending on the strain) and D625 (D624 in EBOV) on the short CHR segment have the capacity to form $i \rightarrow i + 3$ intrahelical interactions (Figure 4D). We previously reported that similar side chain–side chain anionic residues accounted for the pH-dependent stability of the EBOV GP2 six-helix bundle.[28] While surface ionic interactions in coiled coils generally have modest effects, it has been shown in several systems that additive effects of multiple interactions can play a large role in coiled-coil interactions.[41−45]

We generated point mutants of MarVGP2-S and MarVGP2-C at positions 579 and 580 and examined their thermal stability to explore the role of these positions in the pH-dependent stability. The results from these studies are summarized in Table 2. A variant of MarVGP2-C that contained an E580Q mutation at the position predicted to face inward in the core NHR trimer (MarVGP2-CpEQ) was highly unstable at pH 7.0 ($T_m \sim 23$ °C), and a variant containing an E579Q mutation (MarVGP2-CpQE) did not exhibit a strong α-helical signal under these conditions (this position is predicted to interact with E614). These results indicate that neither the E579Q nor the E580Q mutation alone was sufficient to increase the stability at pH 7.0. However, a double mutant containing Glu → Gln mutations at both positions (MarVGP2-CpQQ) had an unusual thermal denaturation profile with at least two transition phases at pH 7.0 (Figure 5). Fitting to a multiparameter logistic

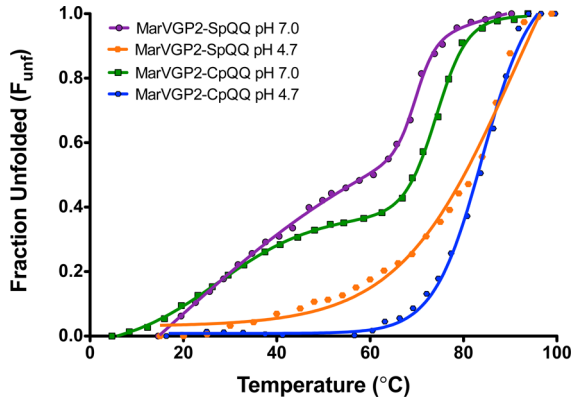

Figure 5. Denaturation profiles of MarVGP2-CpQQ and MarVGP2-SpQQ at pH 4.7 and 7.0.

equation provided two transition temperatures (a minor transition, T_1, and a major transition, T_2) of 27.6 ± 0.5 and 74.0 ± 0.2 °C, respectively. The structural basis of this biphasic thermal unfolding is not clear; in the cases of OmpC and tropomyosin, similar behavior has been interpreted to indicate noncooperative unfolding with each transition corresponding to unfolding of a discrete structural element.[46,47] The first transition in MarVGP2-CpQQ corresponds to approximately 30% of the CD signal, which is equal to the contribution of the CHR segments to the total α-helical content of the EBOV GP2 postfusion structure.[10,11] It is therefore possible that the minor transition corresponds to unfolding of the peripheral CHR segments, and the major transition corresponds to unfolding of the NHR core trimer. At pH 4.7, the MarVGP2-CpQQ clone underwent a single cooperative transition with a T_m of 84.1 ±

Table 2. Summary of Results from Analysis of MarVGP2-S and MarVGP2-C Mutants

variant	mutation(s)	$T_m^{(pH\ \sim 4.7)}$ (°C)[a]	$T_m^{(pH\ 7.0)}$ (°C)[a]	ΔT_m (°C)
MarVGP2-C (WT)	N/A[b]	86.9 ± 0.3	51.6 ± 1.3	35.3
MarVGP2-CpQE	E579Q	ND[b]	(not stable)	–
MarVGP2-CpEQ	E580Q	ND[b]	~23[c]	–
MarVGP2-CpQQ	E579Q/E580Q	84.1 ± 0.9	T_1, 27.6 ± 0.5 T_2, 74.0 ± 0.2	–
MarVGP2-S (WT)	N/A[b]	~88	51.8 ± 0.4	~36
MarVGP2-SpQQ	E579Q/E580Q	81.5 ± 3.5	T_1, 32.2 ± 3.8 T_2, 69.9 ± 0.6	–
MarVGP2-SpKE	E579K	76.9 ± 3.2	~39[c]	~38
MarVGP2-SpEK	E580K	54.8 ± 1.1	~20[c]	~35
MarVGP2-SppQN	E622Q/D625N	83.5 ± 0.4	41.6 ± 2.1	41.9

[a]Errors listed here represent 95% confidence intervals from data fitting. [b]N/A, not applicable; ND, not determined. [c]A broad thermal transition prevented accurate determination of T_m.

dx.doi.org/10.1021/bi3000353 | Biochemistry 2012, 51, 2515–2525

0.9 °C. Similar behavior was observed with a double mutant (E579Q/E580Q) of MarVGP2-S (MarVGP2-SpQQ), though the transition temperatures were somewhat different. These results are consistent with a model in which the E579Q and E580Q mutations serve to stabilize the core NHR trimer at pH 7.0 but have little or no stabilizing effect on the CHR segments.

To further examine the role of residues E579 and E580, we prepared two additional mutants of MarVGP-S: one with an E580K mutation and another with an E579K mutation (MarVGP2-SpEK and MarVGP2-SpKE, respectively). We expected that incorporation of a lysine residue at position 580, which should maintain a positive charge across a broad pH range, should be more destabilizing to global folding stability than an E579K mutation. Indeed, MarVGP2-SpEK was less stable than MarVGP2-SpKE (ΔT_m = 22.1 °C) or MarVGP2-S (ΔT_m = ~33 °C) at pH 4.7. However, both mutants were also less stable than MarVGP2-S at pH 7.0. Together, these results suggest that the pH-dependent stability of the MARV GP2 six-helix bundle is mediated to some degree by E579 and E580.

A variant of MarVGP2-S containing mutations E622Q and D625N on the CHR segment (MarVGP2-SppQN) was also examined (Table 2). This variant had a pH-dependent stability similar to that of MarVGP2-S but was less stable at neutral pH. These results suggest that alteration of these two acidic side chains to their neutral analogues has little effect on the overall pH-dependent stability. Similar surface-exposed side chain−side chain residues were postulated to be important for the pH-dependent stability of α-helical bundle proteins designed from the EBOV GP2 NHR and CHR segments.[28] Therefore, we conclude such interactions play a lesser role in the pH-dependent stability of MarVGP2-S.

DISCUSSION

Characterization of the MARV GP2 Six-Helix Bundle. Here we describe the first characterization of the MARV GP2 ectodomain; we find this segment adopts a stable trimeric α-helical bundle, consistent with the known structures of the phylogenetically related EBOV GP2 and structurally related MoMLV TM ectodomains.[9−11,38] Chemical denaturation indicates that the MARV GP2 six-helix bundle has a folding stability of 33.4 ± 2.5 kcal/mol, which is comparable to the stability of other six-helix bundles involved in viral membrane fusion.[48,49] In the model for membrane fusion involving class I envelope glycoproteins (i.e., those with α-helical ectodomains), folding of a six-helix bundle by the NHR and CHR segments provides the energetic driving force for overcoming the barriers associated with fusing the host and viral membranes.[4−6] Here we show that the relatively short α-helical bundle region of MARV GP2 provides a significant amount of folding energy for this task. We further found that the disulfide bond between C602 and C609 is required for the overall folding stability and therefore likely critical for function.

Implications of pH-Dependent Stability for Membrane Fusion. The folding stability of the MARV GP2 ectodomain six-helix bundle, as estimated by T_m, was greatly dependent on pH, with higher stabilities at lower pH values. We previously reported a similar pH-dependent stability of α-helical bundle proteins designed from the EBOV GP2 NHR and CHR segments.[28] The sensitivity of folding of the six-helix bundle to environmental pH may play a role in the process of membrane fusion. It is thought that the postfusion α-helical bundle is the lowest-energy (ground) state conformation. In the prefusion state, the ectodomain is prevented from adopting the α-helical bundle by interactions with a surface subunit (e.g., gp120 in HIV-1 or HA in influenza A virus).[3−6,21,50] A triggering event releases the constraints on the ectodomain when the viral particle is in a suitable environment for membrane fusion to result in productive viral infection (this model is known as the "spring-loaded clamp" model). The precise molecular events that lead to triggering in HIV-1 gp41 and influenza HA have been established; however, the details of the EBOV fusion pathway are still under investigation. Furthermore, little is known about MARV entry; it is likely the molecular events are similar to those of EBOV given the similarity of their envelope glycoprotein sequences, but biological studies indicate there may be some differences in the entry mechanisms.[17,18] For EBOV, it has recently been shown that NPC1 is critical for entry, and this protein may play a role in the deployment of the GP2 fusion machinery.[15,16]

We and others have suggested that an additional trigger may be endosomal pH, which serves to increase the stability of the postfusion six-helix bundle.[28,36] Furthermore, CatL and CatB have optimal activity at pH ~5, and recent studies also suggest that the fusion loop may itself have some fusogenic properties that are enhanced in lower-pH environments.[29,30] Together, these results suggest that multiple factors involving endosomal resident proteins (NPC1, CatL, and CatB) and endosomal conditions (low pH) work in concert to release constraints on the GP1−GP2 prefusion structure, promote formation of the GP2 postfusion structure, and activate the fusion loop. However, unlike the pH-sensitive transformations observed in influenza HA and SFV E1/E2, in which protonation of specific residues serves to destabilize the prefusion conformation,[19−24] it appears specific protonation events increase the stability of the postfusion conformation. The results shown here provide the first evidence that a similar mechanism for pH-dependent stabilization of the postfusion conformation exists in MARV. Furthermore, mutational analysis suggests the pH-dependent stability is controlled to some degree by acidic residues E579 and E580; the juxtaposition of these anionic residues near other negatively charged residues at neutral pH is predicted to destabilize the postfusion conformation based on the homology model. An accurate description of the side chain−side chain interactions that stabilize and destabilize the postfusion conformation awaits a high-resolution crystal structure of the MARV GP2 ectodomain.

Models for Thermodynamic and Kinetic Control of pH-Dependent Conformational Changes. The dramatic structural rearrangement in the central stalk of influenza HA provides a model for distinguishing mechanisms of pH-dependent conformational changes.[19−21,50,51] A 36-residue segment, which contains a heptad repeat pattern and is predicted to form a trimeric coiled coil, is essentially unstructured and monomeric at neutral pH but adopts a highly stable α-helical bundle at low pH.[21] Baker and Agard proposed two models to describe how environmental pH could have such a dramatic consequence on the overall fold (Figure 6).[51] In the "thermodynamic control" model, the pH affects the relative stabilities of the lowest-energy conformation; at pH 7, the prefusion structure represents the ground state. However, at lower pH, the "fusion active" conformation becomes preferred. A defining feature of this model is that the transition from prefusion to fusion active conformations is reversible, as would be the effects of pH on equilibrium. In the "kinetic control" model, the fusion active conformation is the lowest-energy structure but a high kinetic barrier maintains the prefusion

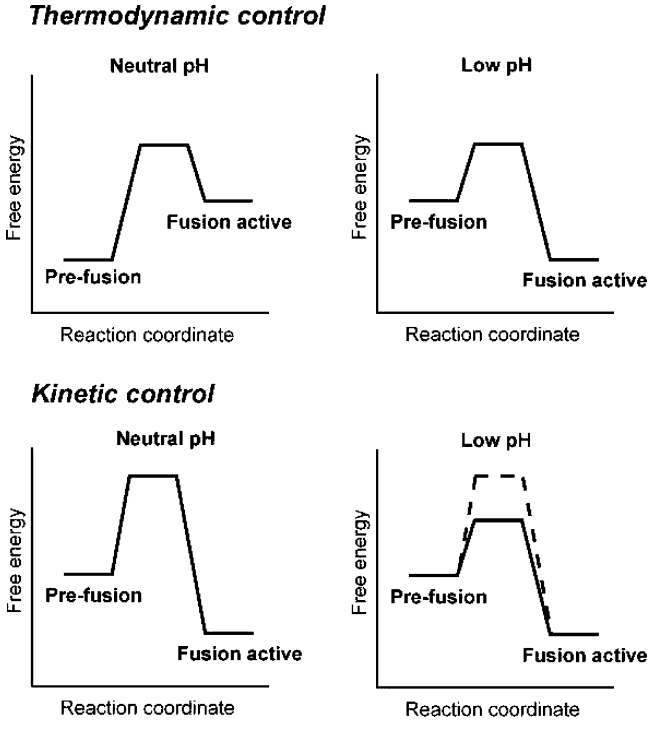

Figure 6. Thermodynamic control and kinetic control models for pH-dependent conformational rearrangements.

conformation. Exposure to low pH decreases the kinetic barrier, facilitating the transition to the lowest-energy (fusion active) conformation. The conformational rearrangements in the kinetic model would be irreversible. Early experiments with HA indicate that exposure to low pH does in fact trigger the pH-dependent conformation on the virus; however, this process is irreversible, which has led to the conclusion that HA obeys the kinetic control model.[3−6,19−21] Furthermore, the fusion active conformation is adopted spontaneously by synthetic peptides corresponding to the core 36-residue segment at low pH,[21] and the fusogenic subunit of HA (HA2) can be refolded into the postfusion structure at neutral pH, suggesting that it is the lowest-energy conformation.[52] These observations suggest the postfusion form is the lowest-energy conformer across all pH conditions.

Other viral membrane fusion proteins, however, appear to exhibit features that are reminiscent of the thermodynamic control model. For example, the envelope glycoprotein G from vesicular stomatitis virus undergoes a pH-dependent transition that appears to be reversible.[25,26] Structural studies suggest that protonations of His residues that are clustered together in the prefusion conformation and of Asp residues that are clustered together in the postfusion conformation shift the equilibrium toward the postfusion conformation.[25,26] The core structural feature of the VSV G low-pH structure is a six-helix bundle (similar to the class I membrane fusion proteins) and includes a number of acidic residues in its proximity. In EBOV, exposure to low pH and mild reductants can trigger the fusogenic properties of the ectodomain on liposomes.[30] However, it is unclear if these in vitro triggers fully recapitulate the in vivo fusion cascade, and it is currently unknown whether such treatments are reversible. We have shown that α-helical bundle proteins corresponding to the ectodomains of EBOV and MARV GP2 have pH-dependent stability;[28] however, these studies have been performed on the isolated proteins alone, and it has not been demonstrated that this behavior is relevant to fusion on a viral surface. Therefore, further experiments on the viral surface are required to establish a model for control of the filovirus GP2 conformational changes associated with membrane fusion.

■ ASSOCIATED CONTENT

Ⓢ Supporting Information

SDS−PAGE analysis of purified MarVGP2-S and MarVGP2-C. This material is available free of charge via the Internet at http://pubs.acs.org.

■ AUTHOR INFORMATION

Corresponding Author

*E-mail: jon.lai@einstein.yu.edu. Phone: (718) 430-8641. Fax: (718) 430-8565.

Funding

This work was funded by the Albert Einstein College of Medicine and National Institutes of Health (NIH) Grants R01-AI088027 (K.C.) and R01-AI090249 (J.R.L.). J.S.H. was supported in part by NIH Molecular Biophysics Training Grant T32-GM008572 and J.F.K. by NIH Medical Scientist Training Grant T32-GM007288.

Notes

The authors declare no competing financial interest.

■ ACKNOWLEDGMENTS

We thank Michael Brenowitz for assistance with the analytical ultracentrifugation experiments.

■ ABBREVIATIONS

MARV, Marburg virus; EBOV, Ebola virus; CatL, cathepsin L; CatB, cathepsin B; NPC-1, Neimann-Pick C1; NHR, N-heptad repeat; CHR, C-heptad repeat; SFV, Semliki Forest virus; IPTG, isopropyl β-D-thiogalactopyranoside; GdnHCl, guanidine hydrochloride; CD, circular dichroism; AU, analytical ultracentrifugation; ASLV, avian sarcoma leukosis virus; THP, tris(hydroxypropyl)phosphine; MoMLV, murine Moloney leukemia virus.

■ REFERENCES

(1) Feldmann, H., and Geisbert, T. W. (2011) Ebola haemorrhagic fever. *Lancet 377*, 849−862.

(2) Kuhn, J. H., Becker, S., Ebihara, H., Geisbert, T. W., Johnson, K. M., Kawaoka, Y., Lipkin, W. I., Negredo, A. I., Netesov, S. V., Nichol, S. T., Palacios, G., Peters, C. J., Tenorio, A., Volchkov, V. E., and Jahrling, P. B. (2010) Proposal for a revised taxonomy of the family Filoviridae: Classification, names of taxa and viruses, and virus abbreviations. *Arch. Virol. 155*, 2083−2103.

(3) Lee, J. E., and Saphire, E. O. (2009) Ebolavirus glycoprotein structure and mechanism of entry. *Future Virol. 4*, 621−635.

(4) Harrison, S. C. (2008) Viral membrane fusion. *Nat. Struct. Mol. Biol. 15*, 690−698.

(5) White, J. M., Delos, S. E., Brecher, M., and Schornberg, K. (2008) Structures and mechanisms of viral membrane fusion proteins: Multiple variations on a common theme. *Crit. Rev. Biochem. Mol. Biol. 43*, 189−219.

(6) Eckert, D. M., and Kim, P. S. (2001) Mechanisms of viral membrane fusion and its inhibition. *Annu. Rev. Biochem. 70*, 777−810.

(7) Lee, J. E., Fusco, M. L., Hessell, A. J., Oswald, W. B., Burton, D. R., and Saphire, E. O. (2008) Structure of the Ebola virus glycoprotein bound to an antibody from a human survivor. *Nature 454*, 177−182.

(8) Dias, J. M., Kuehne, A. I., Abelson, D. M., Bale, S., Wong, A. C., Halfmann, P., Muhammad, M. A., Fusco, M. L., Zak, S. E., Kang, E.,

Kawaoka, Y., Chandran, K., Dye, J. M., and Saphire, E. O. (2011) A shared structural solution for neutralizing ebolaviruses. *Nat. Struct. Mol. Biol. 18*, 1424−1427.
(9) Weissenhorn, W., Calder, L. J., Wharton, S. A., Skehel, J. J., and Wiley, D. C. (1998) The central structural feature of the membrane fusion protein subunit from the Ebola virus glycoprotein is a long triple-stranded coiled coil. *Proc. Natl. Acad. Sci. U.S.A. 95*, 6032−6036.
(10) Weissenhorn, W., Carfí, A., Lee, K. H., Skehel, J. J., and Wiley, D. C. (1998) Crystal structure of the Ebola virus membrane fusion subunit, GP2, from the envelope glycoprotein ectodomain. *Mol. Cell 2*, 605−616.
(11) Malashkevich, V. N., Schneider, B. J., McNally, M. L., Milhollen, M. A., Pang, J. X., and Kim, P. S. (1999) Core structure of the envelope glycoprotein GP2 from Ebola virus at 1.9-Å resolution. *Proc. Natl. Acad. Sci. U.S.A. 96*, 2662−2667.
(12) Chandran, K., Sullivan, N. J., Felbor, U., Whelan, S. P., and Cunningham, J. M. (2005) Endosomal proteolysis of the Ebola virus glycoprotein is necessary for infection. *Science 308*, 1643−1645.
(13) Schornberg, K., Matsuyama, S., Kabsch, K., Delos, S., Bouton, A., and White, J. (2006) Role of endosomal cathepsins in entry mediated by the Ebola virus glycoprotein. *J. Virol. 80*, 4174−4178.
(14) Dube, D., Brecher, M. B., Delos, S. E., Rose, S. C., Park, E. W., Schornberg, K. L., Kuhn, J. H., and White, J. M. (2009) The primed ebolavirus glycoprotein (19-kilodalton GP1,2): Sequence and residues critical for host cell binding. *J. Virol. 83*, 2883−2891.
(15) Carette, J. E., Raaben, M., Wong, A. C., Herbert, A. S., Obernosterer, G., Mulherkar, N., Kuehne, A. I., Kranzusch, P. J., Griffin, A. M., Ruthel, G., Dal Cin, P., Dye, J. M., Whelan, S. P., Chandran, K., and Brummelkamp, T. R. (2011) Ebola virus entry requires the cholesterol transporter Niemann-Pick C1. *Nature 477*, 340−343.
(16) Côté, M., Misasi, J., Ren, T., Bruchez, A., Lee, K., Filone, C. M., Hensley, L., Li, Q., Ory, D., Chandran, K., and Cunningham, J. (2011) Small molecule inhibitors reveal Niemann-Pick C1 is essential for Ebola virus infection. *Nature 477*, 344−348.
(17) Battacharyya, S., Hope, T. J., and Young, J. A. (2011) Differential requirements for clathrin endocytic pathway components in cellular entry by Ebola and Marburg glycoprotein pseudovirions. *Virology 419*, 1−9.
(18) Matsuno, K., Kishida, N., Usami, K., Igarashi, M., Yoshida, R., Nakayama, E., Shimojima, M., Feldmann, H., Irimura, T., Kawaoka, Y., and Takada, A. (2010) Different potential of C-type lectin-mediated entry between Marburg virus strains. *J. Virol. 84*, 5140−5147.
(19) Bullough, P. A., Hughson, F. M., Skehel, J. J., and Wiley, D. C. (1994) Structure of influenza haemaglutinin at the pH of membrane fusion. *Nature 371*, 37−43.
(20) Wilson, I. A., Skehel, J. J., and Wiley, D. C. (1981) Structure of the haemagglutinin membrane glycoprotein of influenza virus at 3 Å resolution. *Nature 289*, 366−373.
(21) Carr, C. M., and Kim, P. S. (1993) A spring-loaded mechanism for the conformational change of influenza hemagglutinin. *Cell 73*, 823−832.
(22) Sánchez-San Martín, C., Liu, C. Y., and Kielian, M. (2009) Dealing with low pH: Entry and exit of alphaviruses and flaviviruses. *Trends Microbiol. 17*, 514−521.
(23) Fritz, R., Stiasny, K., and Heinz, F. X. (2008) Identification of specific histidines as pH sensors in flavivirus membrane fusion. *J. Cell Biol. 183*, 353−361.
(24) Qin, Z. L., Zheng, Y., and Kielian, M. (2009) Role of conserved histidine residues in the low pH dependence of the Semliki Forest virus fusion protein. *J. Virol. 83*, 4670−4677.
(25) Roche, S., Rey, F. A., Gaudin, Y., and Bressanelli, S. (2007) Structure of the prefusion form of the vesicular stomatitis virus glycoprotein G. *Science 315*, 843−848.
(26) Roche, S., Bressanelli, S., Rey, F. A., and Gaudin, Y. (2006) Crystal structure of the low-pH form of the vesicular stomatitis virus glycoprotein G. *Science 313*, 187−191.
(27) Daniels, R. S., Downie, J. C., Hay, A. J., Knossow, M., Skehel, J. J., Wang, M. L., and Wiley, D. C. (1985) Fusion mutants of the influenza virus hemagglutinin glycoprotein. *Cell 40*, 431−439.
(28) Harrison, J. S., Higgins, C. D., Chandran, K., and Lai, J. R. (2011) Designed protein mimics of the Ebola virus glycoprotein GP2 α-helical bundle: Stability and pH effects. *Protein Sci. 20*, 1587−1596.
(29) Gregory, S. M., Harada, E., Liang, B., Delos, S. E., White, J. M., and Tamm, L. K. (2011) Structure and function of the complete internal fusion loop from Ebolavirus glycoprotein 2. *Proc. Natl. Acad. Sci. U.S.A. 108*, 11211−11216.
(30) Brecher, M., Schornberg, K. L., Delos, S. E., Fusco, M. L., Saphire, E. O., and White, J. M. (2012) Cathepsin cleavage potentiates the Ebola virus glycoprotein to undergo a subsequent fusion-relevant conformational change. *J. Virol. 86*, 364−372.
(31) Cantor, C. R., and Schimmel, P. R. (1998) *Biophysical Chemistry, Part II: Techniques for the study of biological structure and function*, pp 426−428, W. H. Freeman and Co., New York.
(32) Boice, J. A., Dieckmann, G. R., Degrado, W. F., and Fairman, R. (1996) Thermodynamic analysis of a designed three-stranded coiled coil. *Biochemistry 35*, 14480−14485.
(33) Pace, C. N. (1986) Determination and analysis of urea and guanidine hydrochloride denaturation curves. *Methods Enzymol. 131*, 266−280.
(34) Schuster, T. M., and Laue, T. M., Eds. (1994) *Modern analytical ultracentrifugation*, pp 3−15, Birkhauser, Boston.
(35) Gallaher, W. R. (1996) Similar structural models of the transmembrane proteins of Ebola and Avian Sarcoma viruses. *Cell 85*, 477−478.
(36) Delos, S. E., La, B., Gilmartin, A., and White, J. M. (2010) Studies of the "chain reversal regions" of the avian sarcoma/leukosis virus (ASLV) and ebolavirus fusion proteins: Analogous residues are important, and a His residue unique to EnvA affects the pH dependence of ASLV entry. *J. Virol. 84*, 5687−5694.
(37) Lau, S. Y., Taneja, A. K., and Hodges, R. S. (1984) Synthesis of a model protein of defined secondary and quaternary structure: Effect of chain length on the stabilization and formation of two-stranded α-helical coiled-coils. *J. Biol. Chem. 259*, 13253−13261.
(38) Fass, D., Harrison, S. C., and Kim, P. S. (1996) Retrovirus envelope domain at 1.7 angstrom resolution. *Nat. Struct. Biol. 3*, 465−469.
(39) Igonet, S., Vaney, M. C., Vonhrein, C., Bricogne, G., Stura, E. A., Hengartner, H., Eschli, B., and Rey, F. A. (2011) X-ray structure of the arenavirus glycoprotein GP2 in its postfusion hairpin conformation. *Proc. Natl. Acad. Sci. U.S.A. 108*, 19967−19972.
(40) Lau, W. L., Degrado, W. F., and Roder, H. (2010) The effects of pKa tuning on the thermodynamics and kinetics of folding: Design of a solvent-shielded carboxylate pair at the a-position of a coiled-coil. *Biophys. J. 99*, 2299−2308.
(41) Kohn, W. D., Kay, C. M., and Hodges, R. S. (1995) Protein destabilization by electrostatic repulsions in the two-stranded α-helical coiled-coil/leucine zipper. *Protein Sci. 4*, 237−250.
(42) Scholtz, J. M., Qian, H., Robbins, V. H., and Baldwin, R. L. (1993) The energetics of ion-pair and hydrogen-bonding interactions in a helical peptide. *Biochemistry 32*, 9668−9676.
(43) O'Shea, E. K., Lumb, K. J., and Kim, P. S. (1993) Peptide 'Velcro': Design of a heterodimeric coiled-coil. *Curr. Biol. 3*, 658−667.
(44) O'Shea, E. K., Rutkowski, R., and Kim, P. S. (1992) Mechanism of specificity in the Fos-Jun oncoprotein heterodimer. *Cell 68*, 699−708.
(45) Lumb, K. J., and Kim, P. S. (1995) Measurement of interhelical electrostatic interactions in the GCN4 leucine zipper. *Science 268*, 436−439.
(46) Keegan, N., Ridley, H., and Lakey, J. H. (2010) Discovery of biphasic thermal unfolding of OmpC with implications for surface loop stability. *Biochemistry 49*, 9715−9721.
(47) Heller, M. J., Nili, M., Homsher, E., and Tobacman, L. S. (2003) Cardiomyopathic tropomyosin mutations that increase thin filament Ca^{2+} sensitivity and tropomyosin N-domain flexibility. *J. Biol. Chem. 278*, 41742−41748.

(48) Jelesarov, I., and Lu, M. (2001) Thermodynamics of trimer-of-hairpins formation by the SIV gp41 envelope glycoprotein. *J. Mol. Biol. 307*, 637−656.
(49) Marti, D. N., Bjelic, S., Lu, M., Bosshard, H. R., and Jelesarov, I. (2004) Fast folding of the HIV-1 and SIV gp41 six-helix bundles. *J. Mol. Biol. 336*, 1−8.
(50) Carr, C. M., Chaudry, C., and Kim, P. S. (1997) Influenza hemagglutinin is spring-loaded by a metastable native conformation. *Proc. Natl. Acad. Sci. U.S.A. 94*, 14306−14313.
(51) Baker, D., and Agard, D. A. (1994) Influenza hemagglutinin: Kinetic control of protein function. *Structure 2*, 907−910.
(52) Swalley, S. E., Baker, B. M., Calder, L. J., Harrison, S. C., Skehel, J. J., and Wiley, D. C. (2004) Full-length influenza hemagglutinin HA2 refulds into the trimeric low-pH-induced conformation. *Biochemistry 43*, 5902−5911.